Opto-Electronics Review

journal homepage: https://journals.pan.pl/opelre

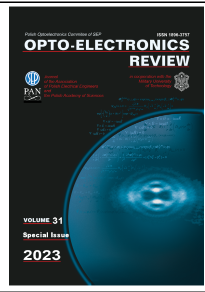

MCT heterostructures for higher operating temperature infrared detectors designed in Poland

Paweł Madejczyk[1*], Waldemar Gawron[1,2], Jan Sobieski[2], Piotr Martyniuk[1], Jarosław Rutkowski[1]

[1] Institute of Applied Physics, Military University of Technology, 2 gen. Kaliskiego St., 00-908 Warsaw, Poland
[2] Vigo Photonics S.A., 129/133 Poznańska St., 05-850 Ożarów Mazowiecki, Poland

Article info

Article history:
Received 27 Sep. 2022
Received in revised form 14 Nov. 2022
Accepted 30 Nov. 2022
Available on-line 24 Feb. 2023

Keywords:
MCT; HgCdTe; metal organic chemical vapour deposition; infrared detectors; higher operating temperature.

Abstract

This paper presents examples of infrared detectors with mercury cadmium telluride elaborated at the Institute of Applied Physics, Military University of Technology and VIGO Photonics S.A. Fully doped HgCdTe epilayers were grown with the metal organic chemical vapour deposition technique which provides a wide range of material composition covering the entire infrared range from 1.5 µm to 14 µm. Fundamental issues concerning the design of individual areas of the heterostructure including: the absorber, contacts, and transient layers with respect to their thickness, doping and composition were discussed. An example of determining the gain is also given pointing to the potential application of the obtained devices in avalanche photodiode detectors that can amplify weak optical signals. Selected examples of the analysis of current-voltage and spectral characteristics are shown. Multiple detectors based on a connection in series of small individual structures are also presented as a solution to overcome inherent problems of low resistance of LWIR photodiodes. The HgCdTe detectors were compared with detectors from III-V materials. The detectors based on InAs/InAsSb superlattice materials achieve very comparable parameters and, in some respects, they are even superior to those with mercury cadmium telluride.

1. Introduction

The traditional HgCdTe infrared (IR) detectors require strong cooling to limit leakage currents and noises originating from thermal generation processes. Many different solutions have been proposed to increase the operating temperature without deterioration of other parameters in higher operating temperature (HOT) detectors extensively researched in scientific centres all over the world [1]. The photodiodes that belong to the group of photon detectors are generally characterised by the highest sensitivities and they mainly determine the IR detector technology development. A fast response and a high signal-to-noise ratio are decisive factors for photodiodes advantage [2]. Despite other alternative technologies, the ultimate properties of mercury cadmium telluride (MCT) ensure that it is the material of choice for all high-performance IR systems [3–4].

CdZnTe substrates are best for HgCdTe deposition due to the perfect match of the crystal lattice. The high cost of CdZnTe substrates and their relatively small available areas necessitate the search for alternative substrates for the HgCdTe growth by the metal organic chemical vapour deposition (MOCVD) method. An inexpensive alternative are GaAs substrates which are easily available in a high-quality and large-size wafers. An inconvenient disadvantage here is the lattice mismatch of 14% between HgCdTe and GaAs that requires the deposition of thick CdTe buffers.

Modern progress in the development of the MOCVD technology created an opportunity for deposition of complex HgCdTe heterostructures with a desired composition and doping profiles. This allows for the design of compound HgCdTe IR detectors dedicated to HOT operation, defined as operating above 200 K. A wide range of different types of IR detectors has been researched, as was shown in the authors' previous papers: photoresistors,

*Corresponding author at: pawel.madejczyk@wat.edu.pl

https://doi.org/10.24425/opelre.2023.144551
1896-3757/ Association of Polish Electrical Engineers (SEP) and Polish Academic of Sciences (PAS). Published by PAS
© 2023 The Author(s). This is an open access article under the CC BY license (http://creativecommons.org/licenses/by/4.0/).

non-equilibrium photodiodes, dual-band and avalanche photodiodes, barrier and multiple detectors [5–6].

The authors present MOCVD-grown HgCdTe heterostructures covering the entire IR range which is conventionally divided into three atmospheric windows: short wavelength IR (SWIR) 1–3 µm, medium wavelength IR (MWIR) 3–5 µm, and long wavelength IR (LWIR) 8–14 µm. In this paper, the authors focus on some fundamental aspects of the design and characterisation of HOT IR detectors from MCT heterostructures. In parallel with MCT, detectors based on III-V materials are also developed in Poland. The detectors based on InAs/InAsSb superlattice materials achieve very comparable parameters to those with MCT.

2. Detectors design

HgCdTe heterostructures are dedicated for IR detectors and in this section some rules of their design will be presented. A classic $N^+/p/P^+$ structure was enriched with the graded gap G layers adjacent to the absorber and they imitate the diffusion of interfaces during the growth in real structure. Furthermore, the structure was upgraded with a p^+/n^+ tunnelling junction to improve electrical contact properties of the metallization with the P^+ layer. The final design took the form of an $n^+p^+P^+G_2\pi G_1N^+$ structure. An example of the HgCdTe detector architecture with a schematic band diagram is presented in Fig. 1.

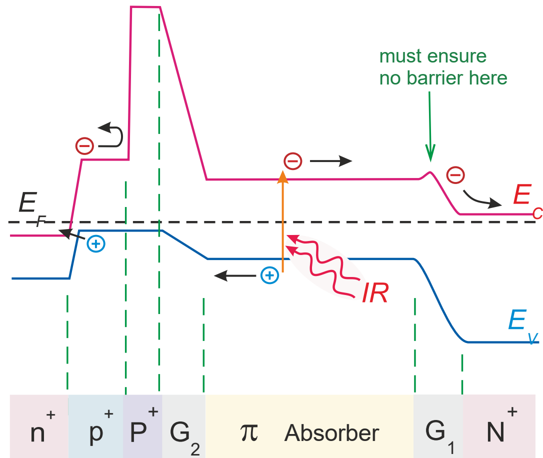

Fig. 1. $n^+p^+P^+G_2\pi G_1N^+$ HgCdTe heterostructure with a schematic band diagram

Considering the order according to the growth direction, the first layer is N^+ (on the right side of Fig. 1). This is a highly doped layer with $N_D > 10^{17}$ cm^{-3} to ensure a low series resistance. The energy gap of the N^+ layer should be wider than that of the absorber region since the structure is irradiated from the substrate side. Thus, the wavelengths to be detected should pass freely through N^+. Next, there is the graded gap region G_1 placed between wide gap – highly donor-doped N^+ and narrow gap – moderate acceptor-doped absorber. Thus, strong grading at this interface concerns both the composition factor – x (of $Hg_{1-x}Cd_xTe$) and the dopants levels, as well. Diffusion processes at the growth temperature determine the energy gap profile. An extremely challenging task for growth engineers is to program G_1 deposition in such way that the resultant interface is devoid of any unwanted potential barrier which may impede the minority carrier flow through the junction (under specific working conditions of the detector). Medium doped p-type absorber region is a central layer of the whole structure. Its doping level is higher than the donor-like background concentration, which is typically of $3\cdot10^{15}$ cm^{-3}. The absorber composition x corresponds to the expected cut-off wavelength of the detector. By selecting the value of the absorber composition x in the range of $0.16 < x < 0.6$, detectors covering any wavelength in the whole infrared range from 1.5 µm to 14 µm can be easily constructed. The absorber should be thicker than the minority carrier diffusion length and is typically of about 3 µm. Graded gap G_2 region separates the wide gap P^+ and the narrow gap absorber. There is a strong grading of the acceptor concentration at this interface. The composition of P^+ layer should be remarkably larger than that of the absorber and the doping should be as large as possible for low concentration of the minority carriers and low resistance. Authors' MOCVD system allows to obtain an acceptor concentration of above 10^{17} cm^{-3}. The thickness of the P^+ layer is about 1 µm. Finally, there is a p^+/n^+ tunnelling junction on the top. An n^+ layer with a donor concentration of about 10^{18} cm^{-3} is applied for low resistance and the composition lower than that of the absorbing region.

3. MOCVD-grown HgCdTe

In accordance with guidelines described in section 2, the $Hg_{1-x}Cd_xTe$ heterostructures were grown in the AIX-200 Aixtron MOCVD system. The system uses a horizontal reactor with the laminar gas flow with process pressures from 50 to 1000 mbar. The pressure was controlled with a butterfly valve. Most of the successful growth runs were carried out at a pressure of about 500 mbar. The diisopropyl telluride (DIPTe) and the dimethyl cadmium (DMCd) were used as precursors, while hydrogen was used as a carrier gas. The tris-dimethylamino-arsenic (TDMAAs) and the ethyl iodide (EI) were used as acceptor and donor dopant sources, respectively. The CdTe buffer layer was deposited on epi-ready, 2 in, (100) GaAs substrates, oriented 2° off towards the nearest <110>. The buffer layer reduces the stress caused by a 14% crystal lattice misfit between HgCdTe and GaAs substrate. Increased composition and thickness uniformities were obtained due to the Aixtron gas foil rotation technique. The HgCdTe epilayers were deposited by the inter-diffused multilayer process (IMP) method. The HgCdTe were grown at 350 °C with a mercury source kept at a temperature of 160–220 °C. *In situ* annealing was carried out under mercury-rich conditions to reduce the residual mercury vacancies concentration and to increase the uniformity of the HgCdTe heterostructures. There was no *ex situ* annealing, however. The HgCdTe growth with the MOCVD technique was extensively studied in Refs. 7–9.

4. Heterostructures characterisation

Vast majority of deposited heterostructures pass through preliminary checking including optical microscopy and IR transmission measurements. Then, they undergo the standard processing procedure which includes

among others: photolithography masking, chemical and ion etching, metallization, cutting, rinsing, electrical connections, and final assembly steps. High purity, diligence, repeatability, and experience of the technical staff play a decisive role in the resultant quality of the constructed detectors. The circular photodiodes with mesa diameters ranging from 30 to 900 µm were formed and mounted on the stands with thermoelectric coolers. The structures were prepared to be back-side illuminated. The presented results concern photodiodes which were not passivated, and no anti-reflection coating was applied. In this section, the selected examples of MWIR and LWIR MCT heterostructures are characterised. Typical issues concerning the specific IR range are given.

4.1. MWIR examples

Figure 2 presents the secondary ion mass spectroscopy (SIMS) profile of the $n^+G_3P^+G_2\pi G_1N^+$ $Hg_{1-x}Cd_xTe$ heterostructure with a composition of x = 0.32 in the absorbing region. This design of the structure, with the research on it, were already published [10]. This is an example of a heterostructure designed for HOT and MWIR operation. The red line represents iodine counts: $8\cdot10^2$ and $2\cdot10^2$ in the n^+ and N^+ regions, respectively corresponding to the designed concentration levels: 10^{18} cm^{-3} and $2\cdot10^{17}$ cm^{-3}, respectively. The abrupt slopes were observed in the iodine profile. A positive consequence is the absence of iodine in the adjacent layers, especially in the absorber region. Theoretically, the N^+ layer should be doped at the highest possible level, which in the authors' case is at the level of 10^{18} cm^{-3} (to ensure low resistance), but the experiments revealed a significant deterioration of the quality of HgCdTe material, if the N^+ doping increases above $4\cdot10^{17}$ cm^{-3}. Dashed blue line represents the arsenic stepped profile corresponding to abruptly changing doses of arsenic in the successive layers: π, P^+, and G_3. Relatively stable arsenic concentration in the absorber region with 6 cts/s corresponds to an expected acceptor level of $6\cdot10^{15}$ cm^{-3}. No undesirable arsenic diffusion to the adjacent layers was observed, so it is a stable dopant. The cadmium, tellurium, and mercury counts allowed to calculate the composition of x profile (the green line) of the entire $Hg_{1-x}Cd_xTe$ heterostructure. Wide energy gap N^+ and P^+ layers with a composition of around x = 0.46 surround the narrower gap absorber with the composition of x = 0.32, as assumed in the heterostructure project. Due to the inter-diffusive processes in HgCdTe material during the growth, the composition profile of the interfaces between the particular layers is graded. This is especially evident in the example of the designed p^+ layer (see Fig. 1) which has completely off diffused creating the graded G_3 region (Fig. 2). A thorough analysis of the SIMS profiles supported by the theoretical calculations allowed adjustments to be made to the programmed growth formulas and allowed to shape the expected profiles in the obtained HgCdTe heterostructures.

One of the potential applications of MWIR HgCdTe heterostructures are avalanche photodiode detectors (APDs). They can amplify weak optical signals, so they are often used in many applications, such as photon counting, light detection and ranging (LIDAR), or astronomy. To determine the gain amount in the obtained heterostructures, a special set of experiments was performed with the current-voltage characteristics measurements in the dark and under illumination. Current-voltage (I-V) characteristics at various temperatures were measured with a Keithley 2400 SourceMeter, controlled via the LabView application for automation. The steady-state photocurrent was generated by radiation from an unfiltered 1000 K blackbody.

Based on these measurements, the avalanche gain G was determined as the ratio of illuminated and dark current difference at certain voltage reverse bias to the same difference at zero bias, according to the following formula [11]:

$$G(V) = \frac{I_{\mathrm{ILLUMINATED}}(V) - I_{\mathrm{DARK}}(V)}{I_{\mathrm{ILLUMINATED}}(V=0) - I_{\mathrm{DARK}}(V=0)} \quad (1)$$

Figure 3 presents the current-voltage plots for the $n^+G_3P^+G_2\pi G_1N^+$ HgCdTe heterostructure for MWIR operation measured at 160 K and 220 K. Mesa diameter is

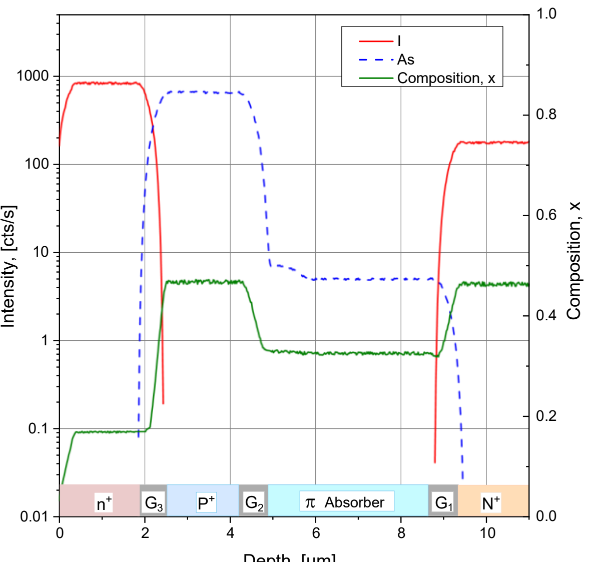

Fig. 2. The SIMS profile of the HgCdTe heterostructure for MWIR operation.

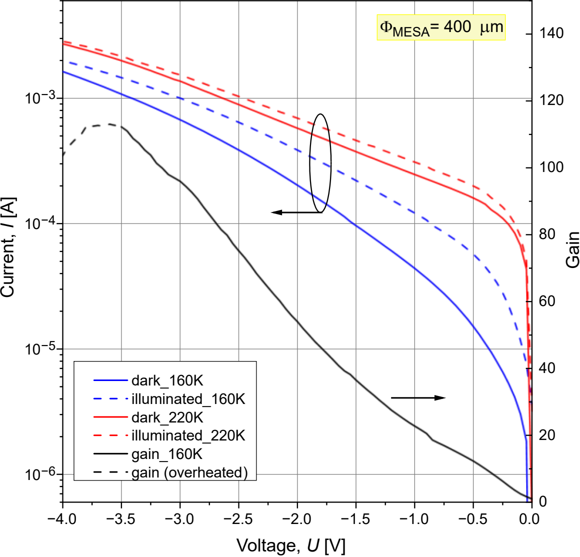

Fig. 3. Current-voltage and gain-voltage plots for the HgCdTe heterostructure for MWIR operation.

400 µm. Figure 3 also shows the corresponding gain *vs*. voltage at 160 K. Gain of 100 was achieved for the moderate bias of −3.5 V what points to some potential application. The temperature control is an extremely fragile issue at this research since the flowing current heats the sample. The rate of uncontrolled heating of the sample exceeds the rate of heat dissipation in the tray. This situation takes place especially when the current rate is above 100 µA during authors' research. The problem is further complicated by the fact that a temperature sensor, which is a calibrated silicon diode, is attached to the holder at a distance of 1 mm from the measured sample. In fact, it is desirable to know the actual temperature inside the measured structure, which is practically impossible. After exceeding −3.5 V, the gain value drops because the sample is overheated (see dashed black line in Fig. 3).

4.2. LWIR examples

Obtained wafers are usually subjected to IR transmission measurements for initial qualification in terms of their spectral range and homogeneity of chemical composition along the wafer.

Figure 4 presents the transmittance characteristics of a randomly selected LWIR $Hg_{1-x}Cd_xTe$ heterostructure measured at different points of the wafer. Measurements were performed using a Perkin Elmer Spectrum 2000GX type Fourier transform IR (FTIR) spectrometer at room temperature. Starting from the central point *a* and then measuring points located along the radius of the wafer: *b*, *c*, *d* (see the inset in Fig. 4) spaced at approximately 8 mm intervals, the authors can estimate homogeneity of the wafer chemical composition. In this case, there is a relatively large gradation of the composition factor x of the $Hg_{1-x}Cd_xTe$ starting with the value of x = 0.1719 at the centre and ending with x = 0.1803 at the edge. Such a large gradation is disadvantageous in the case of arrays design, however, in the case of single detectors this allows for some flexibility in the qualification of individual elements for specific applications. An additional measurement at point *d*1 at the edge and tilted by approximately 90 degrees from point *d* provides information about the actual rotation of the wafer during the growth process. It can be seen that x composition at the point *d* is of x = 0.1803 and at the point *d*1 of x = 0.1804, so the difference of Δx = 0.001 is within the measurement uncertainty, and this is the confirmation that the wafer was really rotating during the deposition process in the reactor (see the curved arrow in Fig. 4).

Equally important conclusions can be drawn based on the current-voltage characteristics of the LWIR HgCdTe heterostructures. Figure 5 presents the current-voltage plots for the LWIR $n^+G_3P^+G_2\pi G_1N^+$ HgCdTe heterostructure measured at different temperatures. The mesa diameter is 100 µm. The negative differential resistance is seen for each of the presented characteristics within the voltage range from −30 mV to −320 mV indicating suppression of Auger processes due to exclusion and extraction phenomena. The threshold voltage, where the Auger suppression begins, increases with increasing temperature. The value of the threshold voltage usually depends on the series resistance and the operating temperature. With a further increase in voltage, the current gradually increases due to the tunnelling or avalanche phenomena. Biasing the photodiode at the threshold voltage provides that the detector resistance is significantly higher than the series resistance even at room temperature, which is more convenient for designing broadband preamplifiers. This is a very good solution for LWIR photodiodes to overcome their perennial disadvantage of low resistance. Increasing photodiode resistance results in a much stronger recovered signal at the amplifier output.

For further device characterisation, spectral response characteristics were studied. Figure 6(a) presents the current responsivity *vs*. the wavelength of the LWIR $n^+G_3P^+G_2\pi G_1N^+$ HgCdTe heterostructure for different temperatures. The mesa diameter is 100 µm. Characteristics were measured with no bias. With the increasing temperature, the current sensitivity decreases as the lifetime of the carriers decreases, which in turn is related to the increasing rate of thermal recombination.

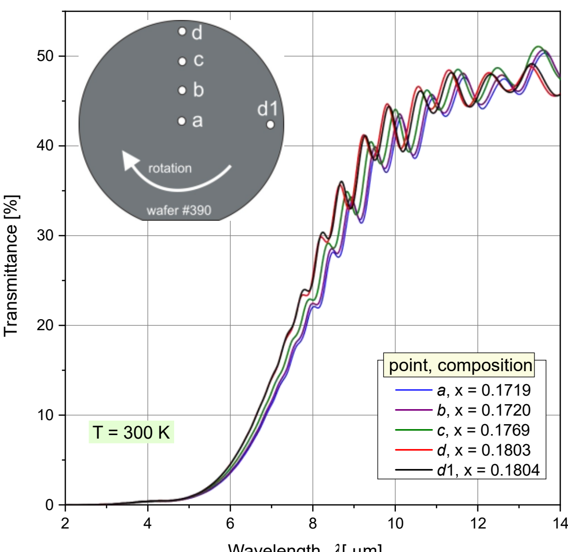

Fig. 4. Transmittance characteristics of the LWIR $Hg_{1-x}Cd_xTe$ heterostructure measured at different points of the wafer.

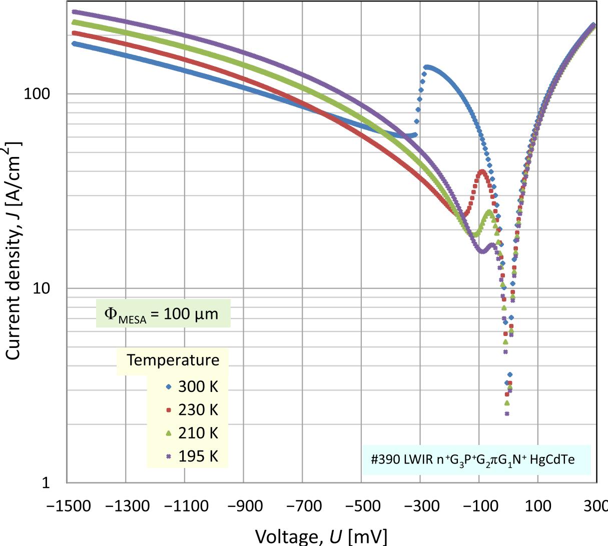

Fig. 5. Current-voltage plots for LWIR MCT heterostructure measured at different temperatures

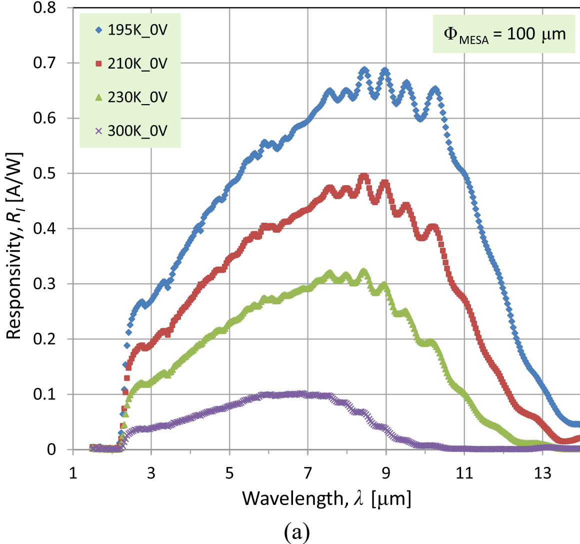

(a)

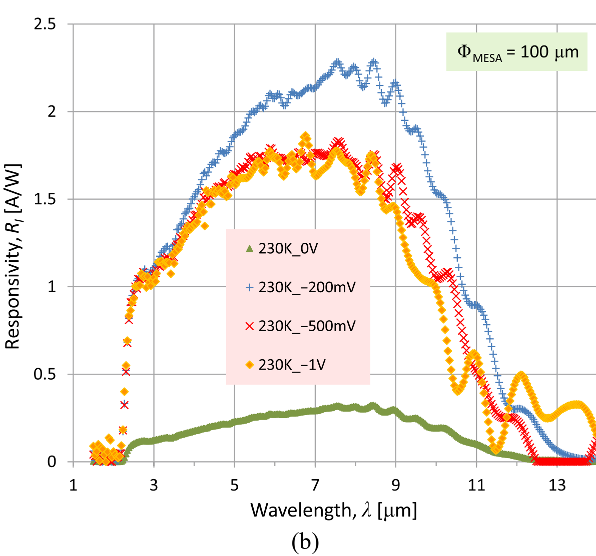

(b)

Fig. 6. Spectral response of the LWIR HgCdTe heterostructure: measured at different temperatures at zero bias (a), characteristics measured at 230 K at different reverse voltages (b).

The cut-off wavelength ($\lambda_{CUT\text{-}OFF}$) is about 8.5 µm at 300 K and about 12 µm at 195 K what qualifies the detector to the group of LWIR devices. The $\lambda_{CUT\text{-}OFF}$ shifts towards shorter wavelengths with increasing temperature, as the energy gap increases (HgCdTe material properties). In turn, the cut-on wavelength ($\lambda_{CUT\text{-}ON}$) is equal to 2.2 µm and determined by the x composition of the N^+ layer. Figure 6(b) presents spectral characteristics measured at 230 K at different reverse voltages. The highest responsivity value $R_I = 2.15$ A/W was obtained for the voltage $U = -200$ mV, because as it results from the I-V curve, the Auger suppression is the strongest at this voltage value.

5. LWIR multiple detectors

Another way to overcame inherent problems of the low resistance of LWIR photodiodes is to connect small individual structures in series integrating multiple detectors in a large area of 4×4 mm^2. In this case, the resultant resistance is simply the sum of resistances of individual cells – see Fig. 7(a). The optimal absorber length is about 2–3 µm, so with this respect the cells should be closely spaced (few microns). However, the presented technology, based on chemical etching and ion-beam milling, enables the repetitive processing with a strips period wider than 10 µm. Multiple detectors period reported in this paper is 20 µm.

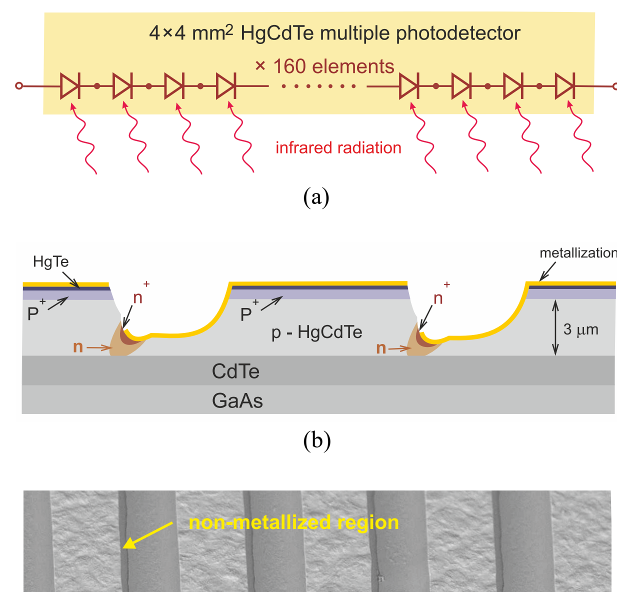

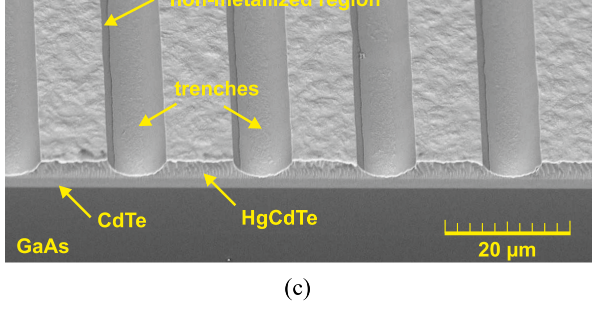

(c)

Fig. 7. Multiple LWIR HgCdTe detector – general idea (a), cross-section draft showing practical implementation of n^+npP^+ junctions (b), and SEM image of real structure taken at a 2800 magnification (c).

Figure 7(b) presents the cross-section draft of multiple LWIR HgCdTe detectors. A pP^+ structure with a total thickness of about 3 µm was obtained using the MOCVD system. Then angled ion etching forms the n^+n regions at selective areas. The n^+ is a strongly damaged region created on the surface of the milled region, and the p to n conversion is due to a diffusion of elements into the p type-doped HgCdTe layer. As a result, the n^+npP^+ photodiode is formed. Device processing technology, rather than fundamental phenomena, determines the size of a single element cell and the cell density. Dynamic resistance and voltage responsivity of multiple photodetectors continue to increase with increasing cell density, even when the absorber length within each cell is shorter than the diffusion length. Figure 7(c) shows a scanning electron microscope (SEM) image of an un-passivated multi-heterojunction HgCdTe photodetector taken at a 2800 magnification. The image shows the structure after the final metallization process. The metallized and non-metallized regions, shapes of trenches, CdTe buffer layer, GaAs substrate, and HgCdTe active layer are clearly seen on the image of this perspective. The trenches depth and the profile uniformity

along the whole structure, the parasitic impedances and the processing repeatability are critical details during the fabrication of multiple photodetectors. These issues have been mostly resolved and large area (1 × 1, 2 × 2, 3 × 3, and 4 × 4) mm² LWIR multiple photodetectors can be fabricated. There are ways for other improvements. One of the solutions is shortening the width of the individual cells below the diffusion length to lower diffusion-limited response time and to rise voltage responsivity.

Figure 8 presents the voltage responsivity and detectivity *vs*. the wavelength of multiple detectors at temperatures of 226 K and 195 K mounted on two- and four-stage thermoelectric coolers, respectively. Measurements were carried out without bias voltage. The physical area of the measured detectors is 1 × 1 mm². The detectors are optically immersed (hyper hemispherical immersion), and the field of view (FOV) is 35 °. The voltage responsivities R_V are 57 V/W and 19 V/W at temperatures of 195 K and 226 K, respectively for the cut-off wavelength of $\lambda = 10.6$ µm. The voltage responsivity continues to increase with decreasing detector temperature, because the quantum efficiency increases due to increasing ambipolar diffusion length of carriers. The obtained detectivity D^* exceeds the level of 10^9 cmHz$^{1/2}$W^{-1} at $\lambda = 10.6$ µm according to the right axis scale. Detector resistances are 175 Ω and 101 Ω at temperatures of 195 K and 226 K, respectively. It is assumed that the uncertainty in the responsivity and detectivity measurement is about ±10%.

Spectral response of LWIR multiple detectors with a 4 × 4 mm² active area without optical immersion of different HgCdTe wafers (different absorber compositions – x_{abs}) is shown in Fig. 9. Measurements were performed without bias voltage at room temperature. The difference in the absorber composition of detectors causes a shift in the cut-off wavelength. The voltage responsivity R_V and the detectivity D^* at the cut-off wavelength of $\lambda = 10.6$ µm exceed values of 0.02 V/W and 10^7 cmHz$^{1/2}$W^{-1}, respectively. The time constants of the presented multiple detectors are below 1.5 ns and the dynamic resistance is in the range from 40 Ω to 100 Ω.

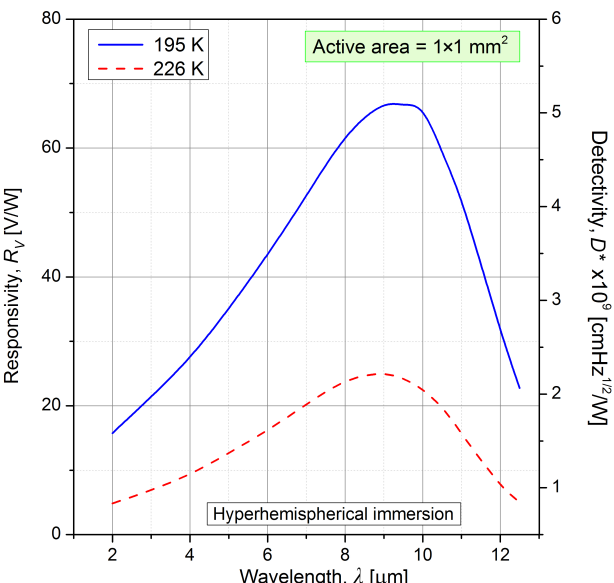

Fig. 8. Spectral response of 10.6 µm cut-off optically immersed multiple detectors mounted on two- and four-stage thermoelectric coolers.

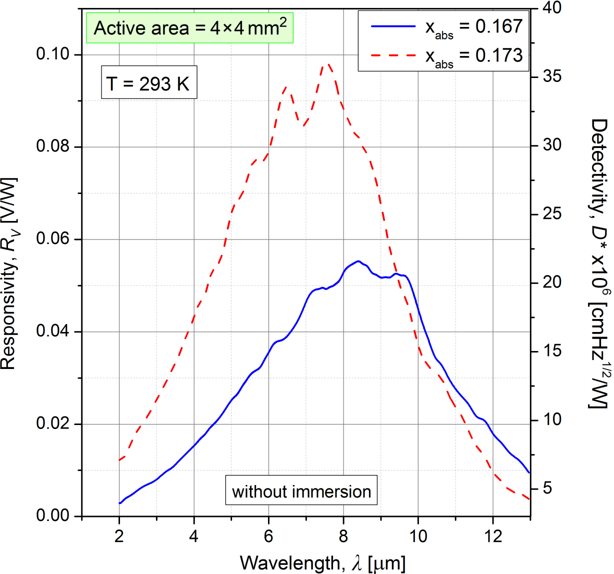

Fig. 9. Spectral response of LWIR multiple detectors at room temperature with 4×4 mm² active areas and without immersion of different HgCdTe wafers.

6. MCT and T2SL comparison

For over 50 years detectors made of HgCdTe material have dominated the infrared industry, as well as related science areas. Competing technologies, however, did not lag far behind, and especially in the last decade they have presented solutions of detection systems with parameters comparable and, in some criteria, even superior to HgCdTe. Detectors of III-V materials with superlattice type II (T2SL) are particularly important. Multicolour detectors and cascade detectors based on InAs/InAsSb are the best examples [12–13].

Figure 10 presents the spectral characteristics of MCT and T2SL detectors for the MWIR range measured at temperatures above 200 K. Both detectors remained unbiased and were without optical immersion. MCT detector is an $n^+G_3P^+G_2\pi G_1N^+$ type structure with

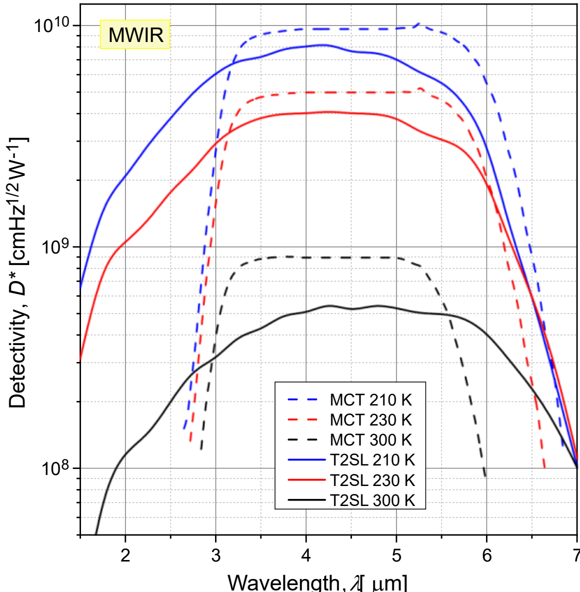

Fig. 10. Spectral characteristics of MCT and T2SL detectors for the MWIR range.

an $Hg_{0.75}Cd_{0.25}Te$ absorber very similar to the one presented in section 4. The T2SL detector is a $p^+B_ppn^+$ type InAs/InAsSb superlattice based on the concept described in Ref. 14. For all three presented temperatures, the MCT detector shows higher values of the detectivity D^* than the T2SL detector by about 20–40%. Considering the measurement uncertainty of detectivity, which is estimated to be about 10% – so the real difference may not be so explicit. A clearly less favourable situation for MCT applies to the LWIR range. Figure 11 presents the spectral characteristics comparison of MCT and T2SL detectors for the LWIR range at 210 K and 230 K. The MCT detector is a multiple LWIR detector presented in section 5. The LWIR SLs inter-band quantum cascade photodetector (ICIP) that achieved D^* of about 2.7×10^8 cmHz$^{1/2}$W^{-1} at 230 K fully confirms its HOT capabilities as demonstrated by Gawron *et al*. [15]. Those comparisons are not entirely authoritative because it is hard to find two detectors of two different technologies with exactly the same shapes of spectral characteristics.

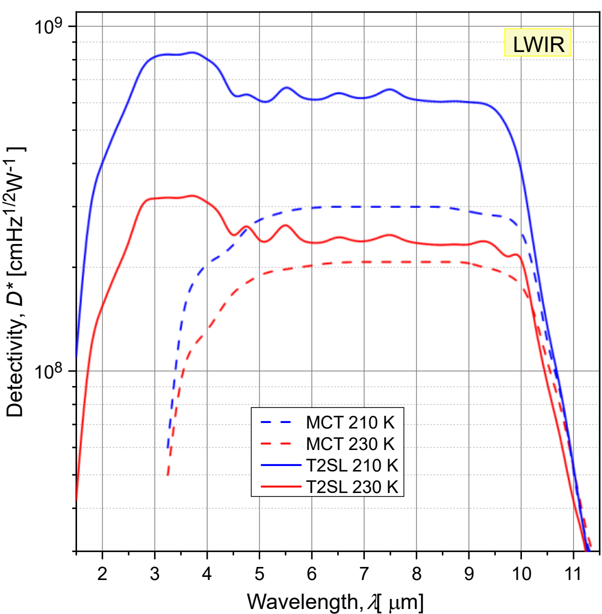

Fig. 11. Spectral characteristics comparison of MCT and T2SL detectors for the LWIR range.

7. Conclusions

The authors presented example issues related to the design and characterisation of MCT HOT IR detectors elaborated in Poland. A wide range of different types of IR detectors operating at HOT conditions has been constructed: non-equilibrium and avalanche photodiodes, barrier and multiple detectors responding to specific market demands. For over 20 years, since the introduction and subsequent optimisation of the MOCVD technology, MCT heterostructures have been systematically improved resulting in better detectors parameters. For example, multiple detector parameters improvement results in an almost ten-fold extension of the optical area, more than a two-fold increase in response speed, increased sensitivity and reduced parasitic series resistance. Despite the dynamic development of competitive technologies, especially superlattices made of III-V materials, MCT maintains a very important position in the infrared industry.

Authors' statement

Research concept and design, P.M. and W.G.; collection and/or assembly of data, J.S.; data analysis and interpretation, J.R.; writing the article, P.M.; critical revision of the article, W.G.; final approval of article, P.M. and J.R.

Acknowledgements

This research was funded by the Ministry of National Defence (Poland), grant no. UGB/22-792/2022/WAT.

References

[1] Kopytko, M. & Rogalski, A. New insights into the ultimate performance of HgCdTe photodiodes. *Sens. Actuator A Phys.* **339**, 113511 (2022). https://doi.org/10.1016/j.sna.2022.113511

[2] Rogalski, A. *Infrared and Terahertz Detectors, Third Edition*. (Taylor & Francis Ltd., 2018).

[3] Kopytko, M. & Rogalski, A. Figure of merit for infrared detector materials. *Infrared Phys. Technol.* **122**, 104063 (2022). https://doi.org/10.1016/j.infrared.2022.104063

[4] Lee, D. *et. al*. Law 19: The ultimate photodiode performance metric. *Proc. SPIE* **11407**, 114070X (2020). https://doi.org/10.1117/12.2564902

[5] Madejczyk, P. *et al*. Higher operating temperature IR detectors of the MOCVD grown HgCdTe heterostructures. *J. Electron. Mater.* **49**, 6908–6917 (2020). https://doi.org/10.1007/s11664-020-08369-3

[6] Gawron, W. *et al*. Multiple long wavelength infrared MOCVD grown HgCdTe photodetectors for high temperature conditions. *IEEE Sens. J.* **21**, 4509–4516 (2021). https://doi.org/10.1109/JSEN.2020.3035246

[7] Maxey, C. D., Capper, P. & Baker, I. M. MOVPE Growth of Cadmium Mercury Telluride and Applications. in *Metalorganic Vapor Phase Epitaxy (MOVPE): Growth, Materials Properties and Applications* (eds. Irvine, S. & Capper, P.) 293–324 (JohnWiley & Sons, Ltd., 2020). https://doi.org/10.1002/9781119313021.ch9

[8] Mitra, P. *et al.* MOVPE growth of HgCdTe for high performance 3–5 µm photodiodes operating at 100–180K. *J. Electron. Mater.* **28**, 589–595 (1999). https://doi.org/10.1007/s11664-999-0040-z

[9] Pillans, L., Baker, I. & Kennedy McEwen, R. Ultra-low power HOT MCT grown by MOVPE for handheld applications. *Proc. SPIE* **9070**, 90701E (2014). https://doi.org/10.1117/12.2050327

[10] Kopytko, M., Murawski, K., Madejczyk, P., Sobieski, J. & Gawron, W. Mid-Infrared HgCdTe heterostructure and its potential application to APD operation. *IEEE Electron Device Lett.* **43**, 761–764 (2022). https://doi.org/10.1109/LED.2022.3159303

[11] Reine, M. *et al.* HgCdTe MWIR back-illuminated electron-initiated avalanche photodiode arrays. *J. Electron. Mater.* **36**, 1059–1067 (2007). https://doi.org/10.1007/s11664-007-0172-y

[12] Razeghi, M., Dehzangi, A. & Li, J. Multi-band SWIR-MWIR-LWIR Type-II superlattice based infrared photodetector. *Results Opt.* **2**, 100054 (2021). https://doi.org/10.1016/j.rio.2021.100054

[13] Michalczewski, K., Jureńczyk, J., Kubiszyn, Ł. & Martyniuk, P. The dependence of InAs/InAsSb superlattice detectors' spectral response on molecular beam epitaxy growth temperature. *Appl. Sci.* **12**, 1368 (2022). https://doi.org/10.3390/app12031368

[14] Gomółka, E. *et al.* Electrical and optical performance of mid-wavelength infrared InAsSb heterostructure detectors. *Proc. SPIE* **10433**, 104330Y-1 (2017). https://doi.org/10.1117/12.2279604

[15] Gawron, W., Kubiszyn, Ł., Michalczewski, K., Piotrowski, J. & Martyniuk, P. Demonstration of the longwave type-II superlattice InAs/InAsSb cascade photodetector for high operating temperature. *IEEE Electron. Device Lett.* **43**, 1487–1490 (2022). https://doi.org/10.1109/LED.2022.3188909